Finite element modelling of a small-size motorcycle for frontal crashes

Finite element modelling of a small-size motorcycle for frontal crashes

Authors: A. Perticone[1,*], S. Meng[2]
[1] Department of Industrial Engineering, Università degli Studi di Firenze, Via di Santa Marta 3, 50139 Firenze, Italy
[*] Corresponding author. Email address: alberto.perticone@unifi.it (A. Perticone); Orcid: https://orcid.org/0000-0003-3170-6746
[2] Autoliv Research, Wallentinsvägen 22, 447 37 Vårgårda, Sweden

Keywords:
Finite-element Modeling
Motorcycle Accidents
Computer Simulation
Crash Analysis
Road Safety

ABSTRACT

Different from passenger car safety, Powered Two-Wheeler (PTW) crashworthiness analysis is not systematic, and no legal requirements prescribe how to test full vehicle PTW safety. The only existing guidance is provided in ISO 13232; it prescribes computer modeling but mainly for Multi-Body models and lacks some essential aspects for Finite Element (FE) models. The aim was to develop an FE model of a small (<150 cc) PTW for frontal crashes.
In a reverse engineering process, a Yamaha YS-125 was disassembled and scanned to establish a basis for virtual modeling in LS-DYNA FE code. Analysis of physical crash tests guided which frontal structures were critical to replicate PTW dynamic responses and rider-to-PTW interactions. Two physical tests were conducted and replicated numerically: a frontal crash of the PTW into a rigid barrier and a frontal crash into the side of a Honda Accord, including the Autoliv-Humanetics PTW dummy as a rider.
The scanned base model included five critical components in more detail: the front wheel, front suspension, headlamp, handlebar, and fuel tank. Precisely, tire pressure and rim failure mechanism were replicated; spring/damping characteristics of the suspensions and fork bending were adapted; handlebar and headlamp rotations were modeled; and fuel tank interaction with the pelvis was replicated. With these components correctly modeled and assessed, the developed PTW model is predictive of PTW and rider accelerations and motion during frontal crashes. These findings are a starting point for modeling safer motorcycles and defining regulations that standardize modeling techniques and validation of FE models.

1 Introduction

Powered Two Wheelers (PTW) crashworthiness analysis is not systematic [1]. Even today, there is a lack of international standard procedures required to test motorcycles during crashes. The International Organization for Standardization (ISO) developed "test and analysis procedures for research evaluation of rider crash protective devices fitted to motorcycles" in 1996 and revised it in 2005 [2]. It covers aspects of conducting physical crash tests for motorcycles [3] and procedures for performing computer simulations [4], but it is not a legal requirement to comply with ISO to validate a PTW model or test.
It is claimed that ISO was conceived "regardless of whether the multi-rigid body, finite element (FE) or other emerging methods are used" and that "efforts were made during the development of the Standard to ensure that […] either MB or FE techniques could be used" [5]. In particular, the ISO demands only two static and three dynamic tests for the PTW, accounting for the fuel tank, seat, and rear spring damper. Besides, a full barrier test is also demanded to observe: the PTW center of gravity displacement, PTW pitch angle, front suspension compression, and fork bending. Although the Standard is not intended to be a workbook to solve CAE problems (instead, it ensures minimum levels of detail so that the results may be relied upon), it became

apparent concerning the abovementioned tests that the ISO 13232 has to be assumed, at least, outdated for the way it addresses the FE needs, despite its revision in 2005. Moreover, along the Standard, many words and concepts indirectly refer to the multi-body environment. The experimental tests are intended to derive forces and deflection, which are the essential responses to define contact characteristics in MB models, but on the opposite, they are not readily usable in FEs. These motivations suggest that the Standard is more disposed to rigid body simulations [6]. Therefore, the question of how to model a PTW remains an active area of research, and this paper aims to make a contribution toward answering it. To this end, a comprehensive review of existing literature was conducted, with the goal of identifying various approaches and considerations relevant to the development of a computer model for a PTW.

To the authors' knowledge, the first attempt to develop vehicle models was published in the early 70s by the National Highway Traffic Safety Administration, and it consisted of a five-mass rider and a single-mass motorcycle [7]. Some early developments with lumped mass and multi-rigid components followed in the 80s in a Ph.D. dissertation [8] and some works from the Transport Research Laboratory (TRL) [9]. The complexity of the models increased quickly, so in the 90s, pioneering works on multibody modeling were published worldwide: such as those by the TRL [10], TNO Crash-Safety Research Center [11,12], Dynamic Research [13], Japanese Research Institute [14] and eventually Honda [15], where the first hybrid FE/multibody interaction appears in the case study of an airbag model. As the new century dawned, hybrid models became increasingly popular for their capacity to reproduce deformations rather than just predicting trajectories and forces. The finite element technique was more accurate but still demanding regarding simulation time and computer resources. Therefore, these models typically had a deformable (i.e., FE-based) frame and most of the contact surfaces, but still, many components were simplified or not modeled at all. This way of implementing FE turned out to be effective, and its popularity spread in the first decade of the new century also thanks to commercial software, such as PAM-CRASH [6,16–18] and MADYMO [19–24]. Computer simulations required enormous efforts to provide results, and in that decade, very few were attempts via explicit software, such as LS-DYNA [25,26]. Differently, from 2010 to date, FE PTW models acquired central visibility [1,27–32], but they did not replace their hybrid/multibody simplified counterparts [33–44]. Some authors preferred to adopt the multibody approach because they were either not interested in the stress/strain outcomes or involved in an extensive campaign of simulations, such as parametric studies. Many of the above-cited papers referred to ISO 13232 to validate their PTWs, and, as a common practice, the authors considered either a visual comparison of the global motion or quantitative responses like accelerations and forces or a mix of them. Even in the works where FEs are implemented, the modeling considerations are sparse and not comprehensive of every component and their mutual interaction. While it can be reckoned satisfactory for many multibody implementations, a comprehensive view is vital when FEs reply to multibody vehicles since each part can interact with the others. In addition, a closer look at the FE is felt urgent as the evolution from multibody to finite element models was made possible by the ever-growing computational speeds and the level of details of commercial software so that nowadays, FEs are more used than ever. Therefore, developing an FE model of PTW, this paper addresses the fundamental components to consider simultaneously when FE PTW models are implemented for frontal crash purposes.

2 Method

2.1 PTW modeling

2.1.1 Reverse engineering process

Frequently, geometry and material data of motorcycles are a company's confidential information and hence not publicly available. When it happens, a reverse engineering technique is generally adopted to develop the computer model [18,29,43,45,46].

The Yamaha YS125 was chosen as representative of the Asian market, which is the largest PTW market worldwide with approximately three-quarters of the global fleet, a considerable portion of which is covered by small-engine (<150 cc) motorcycles [47]. Hence, it was chosen as PTW for both simulations and tests, Figure 2.1. A 3D FARO arm scanner has been used to scan each part of the PTW. Before scanning, every

component was weighted, and a coarse estimation of the material family was made. Once the 85 scans were completed, Computer-Aided Design (CAD) parts were available and refined to be set as FE models in LS-DYNA. First, the mesh was created, material and property attributed, and then a computer weighting was done to compare the fictitious mass with the physical counterpart. In those cases where the two measures differed, a lumped mass was added to the virtual part. All these parts were combined with reference to the frame to complete the computer model. Eventually, the overall wet weights were measured in the two models and compared. Since the computer model still had a lower mass than the physical one, as many parts were not considered (e.g., cables, oils, fuel, screws, and bolts), a lumped mass was added in a specific position so that the final center of gravity (CoG) should match. This procedure required a confident knowledge of the original CoG, measured in this study with the traditional methodology [48].

Figure 2.1 – The Yamaha YS125 obtained with the reverse engineering process (left) and the actual one (right)

2.1.2 Front-wheel

Each part of the wheel was first measured with the caliper, then scanned and meshed in shell elements, Figure 2.2. The thickness of the tire was measured twice on the tread and the side wall; then, a hyperelastic rubber was defined via the Mooney-Rivlin material model. The input parameters of the energy strain tensor function were taken from similar tire applications in literature [49–54] and slightly increased since the layers that typically compose a tire (such as nylon, polyester, steel cords, and fabric) were not included in this case for simplicity, Table 2.1. The material for the rim was taken from the online Yamaha OEM sheets, which indicated a Japanese AC4CH aluminum casting alloy or, equivalently, the A356.0 aluminum in the Aluminum Association's (AA) nomenclature with a T6 temper. Its mechanical behavior was modeled in LS-DYNA via the MAT_PIECEWISE_LINEAR_PLASTICITY card. The bead was modeled to reinforce the tire at the rim. It usually helps transmit the torque to the wheel, but in this case, it also prevents numerical error caused by the pressure inside the tire after the rim breaks. AIRBAG_SIMPLE_PRESSURE card was exploited to simulate a pressurized tire. It was assumed no air leakages (neither venting nor porosity) and that the influence of the temperature to tire pressure was negligible. Values of 200 kPa and 220 kPa were first measured with the pressure gauge and then implemented for the front and rear tires, respectively.

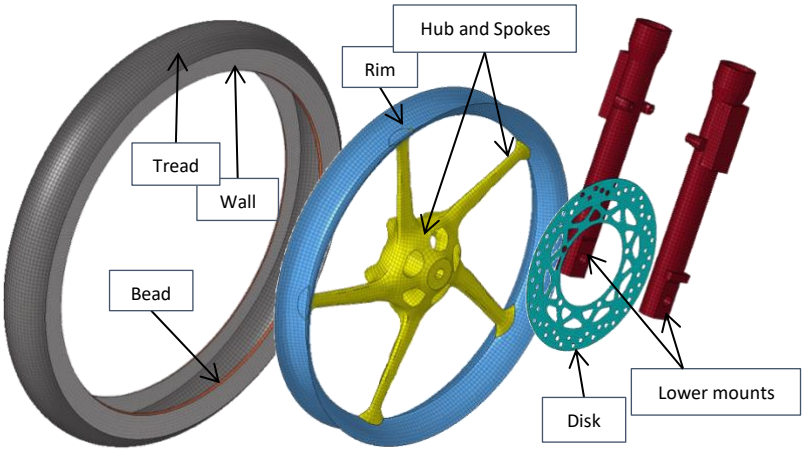

Figure 2.2 - Front-wheel components

Parts	Thickness [mm]	Material	Parameters [MPa]	Parameters [MPa]
Tread	9.0	Rubber	C_{10} = 10.1	C_{01} = 10.1
Sidewall	6.0	Rubber	C_{10} = 10.8	C_{01} = 10.2
Bead	8.0	Aluminum	σ_y = 201	E_{tan} = 1580
Rim	8.0	Aluminum	σ_y = 201	E_{tan} = 1580
Hub and Spokes	6.5	Aluminum	σ_y = 201	E_{tan} = 1580
Lower mounts	4.0	Aluminum	E = 70000	–
Disk	3.0		E = 210000	–

Table 2.1 - Materials and properties of the wheel

2.1.3 Suspensions

Generally, a motorcycle suspension is composed of a telescopic fork and a lower mount (or leg), which hosts it, both connected to the steering stem through a pair of triple clamps that provide a tight fit. Different materials were used for suspensions: steel on forks and aluminum on legs, Table 2.2. For the latter, the Yamaha OEM website reported either a Japanese AC2B or AC4C aluminum alloy, but in this case, the component was kept elastic, assuming no plasticity for it [55]. In standard industry practice, the forged triple clamp is commonly made of C20 carbon steel [55]. The stress-strain curve was implemented with the MAT_PIECEWISE_LINEAR_PLASTICITY card after selecting it from [56]. The leg and fork were modeled by shell elements and joined together via a CONSTRAINED_JOINT_CYCLINDRICAL element that ensured relative rotation and translation along the centerline. The two joints were defined only at the shaft lower extremity to avoid the stiffening that would have resulted if the joints had been put along the whole fork.

Parts	Thickness [mm]	Material	Parameters [MPa]	Parameters [MPa]
Fork shaft	3.5	Steel	E = 210000	σ_y = 900
Lower mount (leg)	4.0	Aluminum	E = 70000	–
Triple clamp	6.0	Steel	E = 210000	σ_y = 455

Table 2.2 - Materials and properties of the suspensions

Likewise significant in a suspension system are the damper and the spring inside, which determine its response. These components were modeled using two one-dimensional overlapped discrete elements for each fork. Ten repetitions of a quasi-static test were performed to measure the spring rate, which resulted in 1.0 kg/mm stiffness before the bottom out at 120 mm. This response was shifted in LS-DYNA by the length of which the front fork was pre-compressed by the PTW itself (plus the dummy on it, if any). This initial pre-compression was measured in the physical model, and extra 150 ms was left with the card

INITIAL_VELOCITY_GENERATION_START_TIME to allow the suspension system to reach an equilibrium point in the computer model. The rear suspensions were also modeled, even though they do not get involved in the frontal crash, to reach the correct final height from the ground.
On the other hand, the damping values were not measured but assumed. A bilinear behavior in rebound and a softer compression were implemented with damping *MAT_DAMPER_NONLINEAR_VISCOUS elements in LS-DYNA, Figure 2.3.

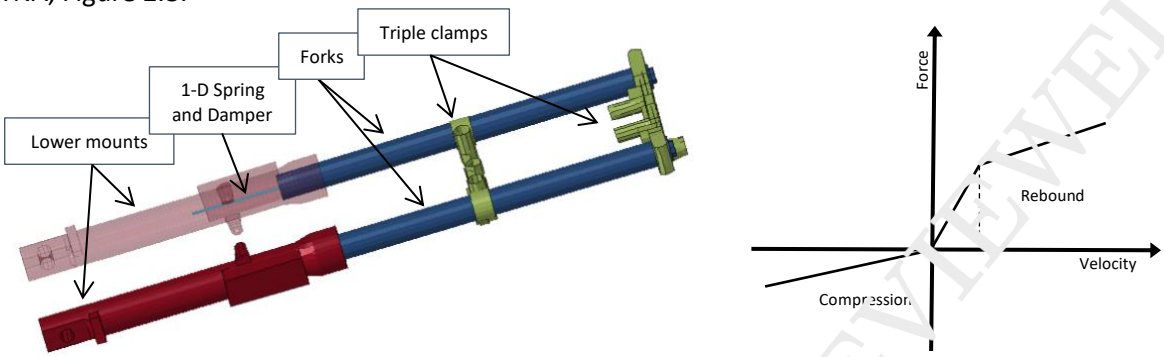

Figure 2.3 – On the left hand, the suspension scheme. On the right hand, the response implemented in LS-DYNA.

2.1.4 Headlamp, handlebar, and tank

The headlamp was equipped with three rotational joints since it is a prominent part of the PTW likely to hit the OV in a frontal crash, Figure 2.4.
Analogously, the handlebar was left free to rotate inside the clamps. However, in this case, the geometry guaranteed the rotation: a dedicated friction contact was created between the clamps and handlebar, and the geometry was accurately refined, avoiding interferences, and self-node penetrations, Figure 2.4.
Eventually, the tank was physically cut to measure the inner thickness (1 mm). The position of the trims was double-checked after the 3D scansion and manually repositioned to avoid interactions with the dummy. The material was not tested but assumed and calibrated to reproduce the correct interaction with the dummy ($E = 210000$ MPa, σ_y = 450 MPa, E_{tan} = 1300 MPa).

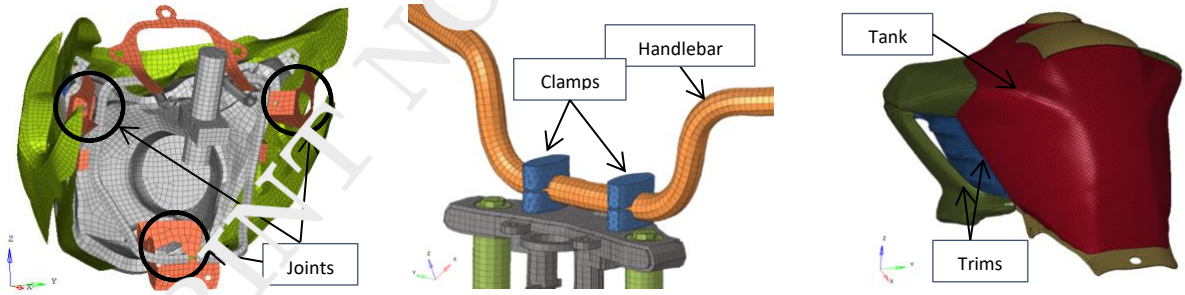

Figure 2.4 – From the left to the right side: the headlamp, the handlebar, and the fuel tank.

2.2 Test and simulation setup

Two test setups were simulated and compared to their physical tests: the first one represented a rigid barrier test, i.e., a crash between a motorcycle and an instrumented concrete block, with neither riders nor passengers; the second simulation represented a full crash test with the PTW hitting the panel door of an opposite vehicle (OV) perpendicularly, Figure 2.5. In the full crash test, 50 km/h was the selected impact speed since it is known that the sensitivity at small perturbations in computer models increases with impact speed, making simulation uncertain at velocities greater than 56 km/h [10]. Similarly, the rigid barrier test was performed at 40 km/h, knowing that, given the high stiffness of the barrier, a comparable level of deformations on the PTW could be achieved at lower velocities.

The PTW was instrumented with four accelerometers: two were placed on the forks to monitor the wheel acceleration, one on the bottom of the engine block, and the last one on the upper rear frame, under the saddle. To acquire the response of the front wheel, the right and left fork accelerations were post-processed with an average operation. In the full crash test, one more accelerometer was placed on the upper triple-clamp near the steering column. All the signals were filtered with the SAE J211 CFC 60 filter. Time zero was marked at the first contact with the wheel and the barrier or the OV.
The Honda Accord was the stationary OV for the full crash test, available online in the NHTSA's archive as the model year 2011. The virtual vehicles were positioned on the ground, and a friction coefficient of 0.7 was set for contact with the vehicle tires, in agreement with other works [38,39,41]. In the rigid barrier test, a specific friction coefficient of 0.6 was set for the contact between the PTW front wheel and the barrier, according to [17]. Depending on the test, a static and dynamic friction coefficient of 0.3 was supposed for the contact between the PTW and the car or the barrier. A constant field of gravity was imposed for every model.

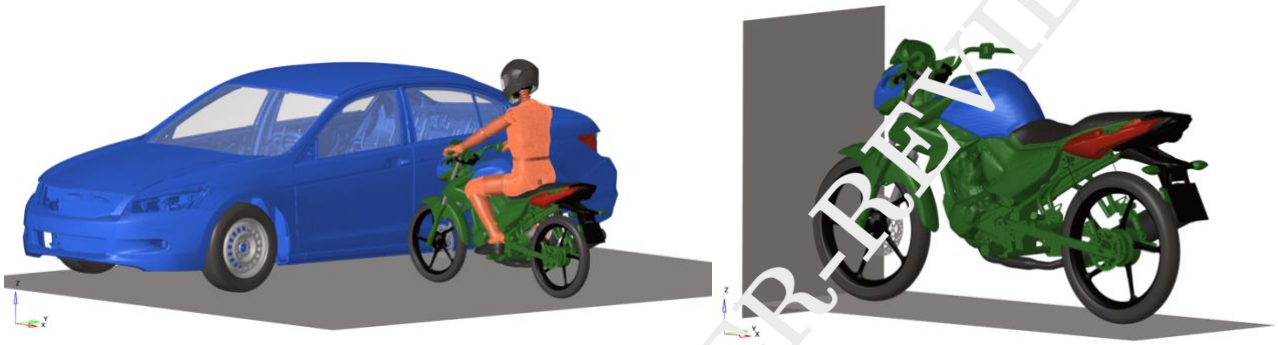

Figure 2.5 – Full crash simulation (left) and rigid barrier test (right)

The Autoliv-Humanetics PTW dummy model, version 1.0.1, was chosen as the rider for tests and simulations since the development of the PTW riding dummy has paired physical and FE models together [57]. Pre-test measurements were made along several points to get the closest position possible between the virtual and the physical dummies. The measured parts were H-point, shoulders, knees (both foremost fleshes and joints), pelvis accelerometer slot, chin, and helmet center. The "marionette method" [58] was used to position the virtual dummy on the PTW and implemented in three steps.
Depending on the length of physical tests, the run time was set to capture all the motion until either the PTW rebounded on the rigid barrier or the rider hit the OV. In both cases, a pre-simulation was introduced seamlessly before the models started moving, depending on the time needed to set the models. Its primary purposes were 1) to allow moveable parts (like joints, e.g., the front and rear suspensions) to reach their dynamic equilibrium, as described in paragraph 2.1.3; 2) to allow deformable parts to be adequately pre-stressed (like foams, e.g., the saddle cushion and the helmet liner); 3) to allow the entire model to get contacts activated (e.g., wheels to the ground or hands on the handlebar).

3 Results

The following paragraphs will demonstrate the predictive capacity of the described computer model in replicating the signals, motion, and main deformations of its physical counterpart in two laboratory tests.

3.1 Rigid barrier test

Figure 3.2 compares the overall motion between the test and simulation. In the last picture of Figure 3.2, the measurement of the whole rebound was reported to show that the quantity of dissipated energy was comparable between the test and simulation since the two rebounds measured both about one meter.
At 8 ms, the front tire was completely squeezed against the rigid barrier. The accelerometers on the forks recorded the first deceleration peak, Figure 3.1. At 10 ms, the front wheel started rising off the ground, lifted by the compression of the front suspensions. The compression depleted quickly, and before 15 ms from the

first contact, the front forks started bending while the rest of the PTW continued moving forward. This motion caused the first positive peak. At 20 ms, the engine bracket (the metal plate that joints the frame's front pipe with the engine) touched the back side of the wheel. At 25 ms, the tire was compressed entirely, and the bracket loaded the rim. At this time, a negative acceleration of about 50 g was recorded similarly on the forks, engine, and rear frame. After 25 ms, all the accelerations consistently decreased up to 60 ms, when they finally settled around zero. The FE simulation predicted the acceleration/deceleration peaks that coincided with the experiment, hence captured these phenomena. However, the peak acceleration/deceleration magnitude was higher in the simulation than in the experiment. Interestingly, acceleration/deceleration measured at the engine block and rear of the upper frame showed a single deceleration pulse. The engine deceleration predicted from the simulation had good agreement with the experiment in terms of peak value and pulse shape.

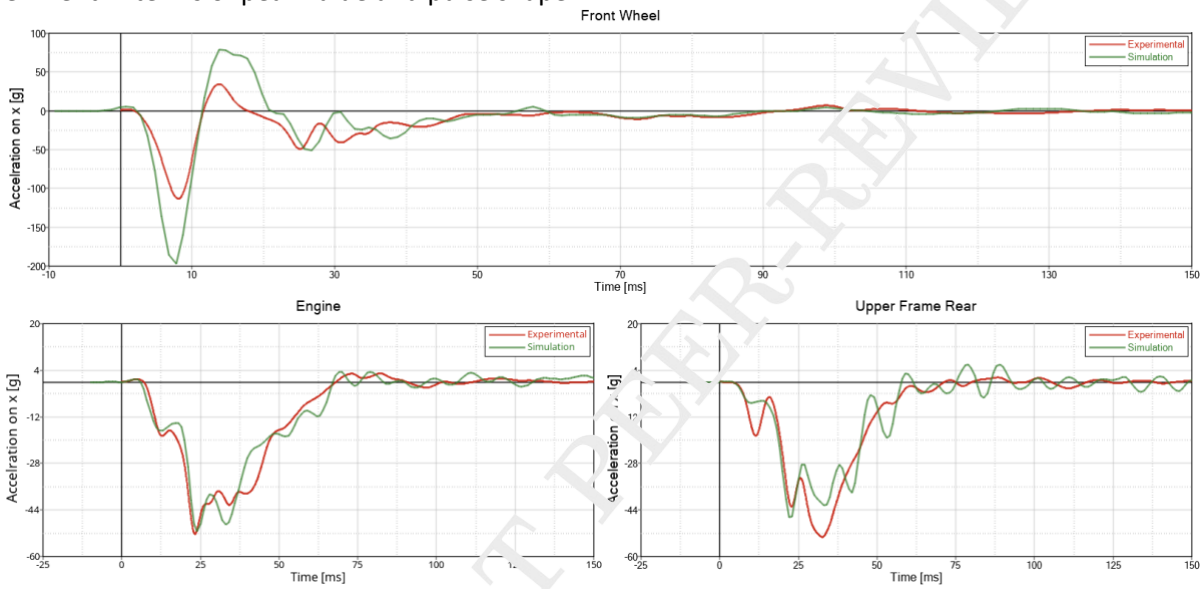

Figure 3.1 – The acceleration-time history measured at the frontal wheel, engine, and the rear of the upper frame from the rigid barrier test (red) and the simulation (green)

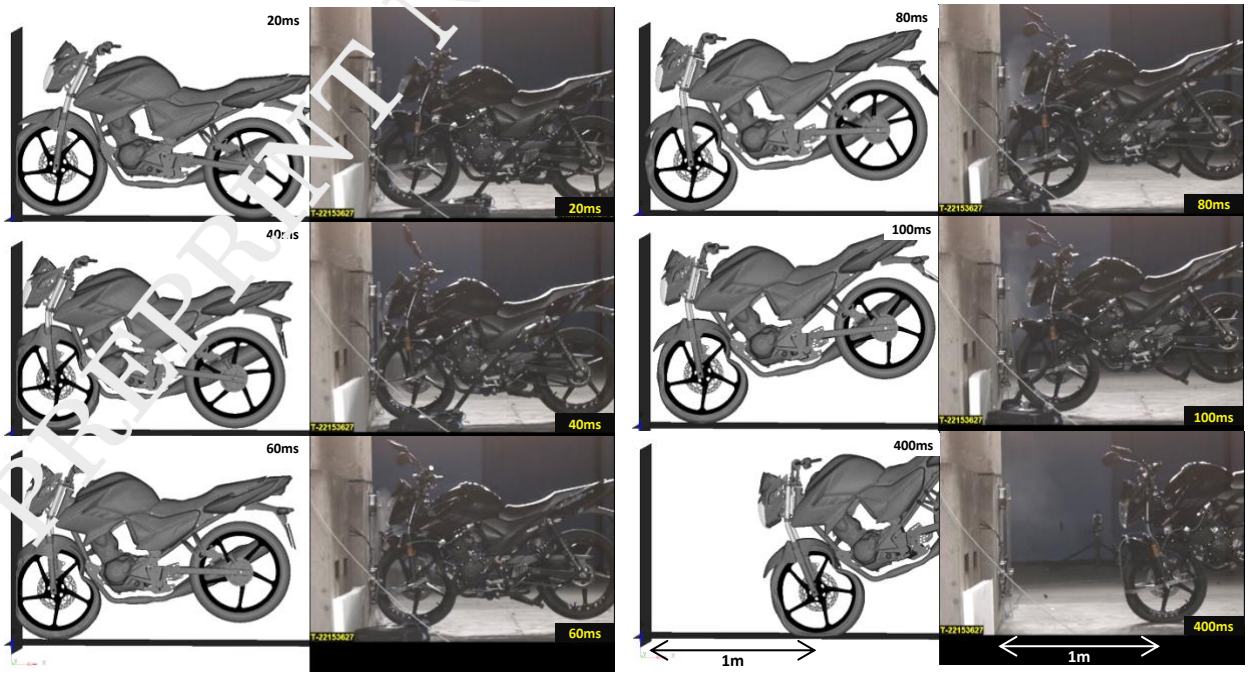

Figure 3.2 - Motion comparison between the computer model (left) and the rigid barrier test (right)

3.2 Full crash test

The PTW hit the OV with the front wheel at time zero, Figure 3.3. Up to 10 ms, neither failure nor permanent deformations were visible on the PTW, while the lateral panel door showed plastic deformations. Before 15ms from the first contact, the front forks started bending, turning to be the first permanently deformed parts on the PTW, Figure 3.4 (left). At 20 ms, the back side of the front wheel was reached by the engine bracket, and, in 20 ms more, it broke the wheel rim between two spokes while leaving them not visibly bent or permanently deformed, Figure 3.5. At 25 ms, the headlamp started touching the car door, first rotating around its joints, then collapsing between the two vehicles, Figure 3.6. At 30 ms, the dummy started sliding on the saddle and pushing the tank for 20 ms. At 40 ms, after the rim failure, one spoke indented the front pipe of the frame above the engine bracket, Figure 3.4 (right). At the same time, the handlebar started rotating inside the clamps, pushed forward by the weight of the dummy. Although the hand grasp differed from the one in the test, Figure 3.6, the contact was still held way after the contact between the PTW and the OV. Around 50 ms, the PTW started pitching forward, Figure 3.3. At 60 ms, the handlebar was completely rotated inside the clamps, and the hands touched the window. At this time, the dummy started lifting and left contact with the saddle. Twenty ms later, the pitch increased, and the dummy continued its motion against the OV, with the abdomen contacting the fuel tank and legs extending. At 100 ms, the helmet's visor hit the OV trail, and head contact occurred while the front tire separated from the panel door. All the same motions and deformation mechanisms were captured with the computer model. In addition, the fuel tank was noted to deform after 30 ms when the dummy started sliding on the saddle. This deformation also happened during the test, but the timing was not confirmed because cameras and sensors did not catch it.
Figure 3.7 reported the comparison of acceleration curves between the simulation and experiment. The same as in the rigid barrier test, the first negative peak originated from the interaction between the front wheel and the OV; the first positive peak was caused by the rest of the PTW moving forward; the second negative peak corresponded to the load of the rest of the PTW moving against the front wheel. Eventually, the second positive peak, new in this test, was due to the mass of the dummy pushing forward on the fuel tank and the handlebar. The engine and the rear upper frame recorded a consistent trend in magnitude and timing to those reported in the rigid barrier test. The steering column recorded the smoothest signal without any peaks. Comparison for acceleration-time history between FE simulation and experiment showed an overall good match of the peaks in amplitude and timing. The engine and steering responses predicted from the simulation had the best agreement with the experiment. However, the front wheel and the rear frame also captured the phenomena and closely resembled the experiment in terms of peak and timing.

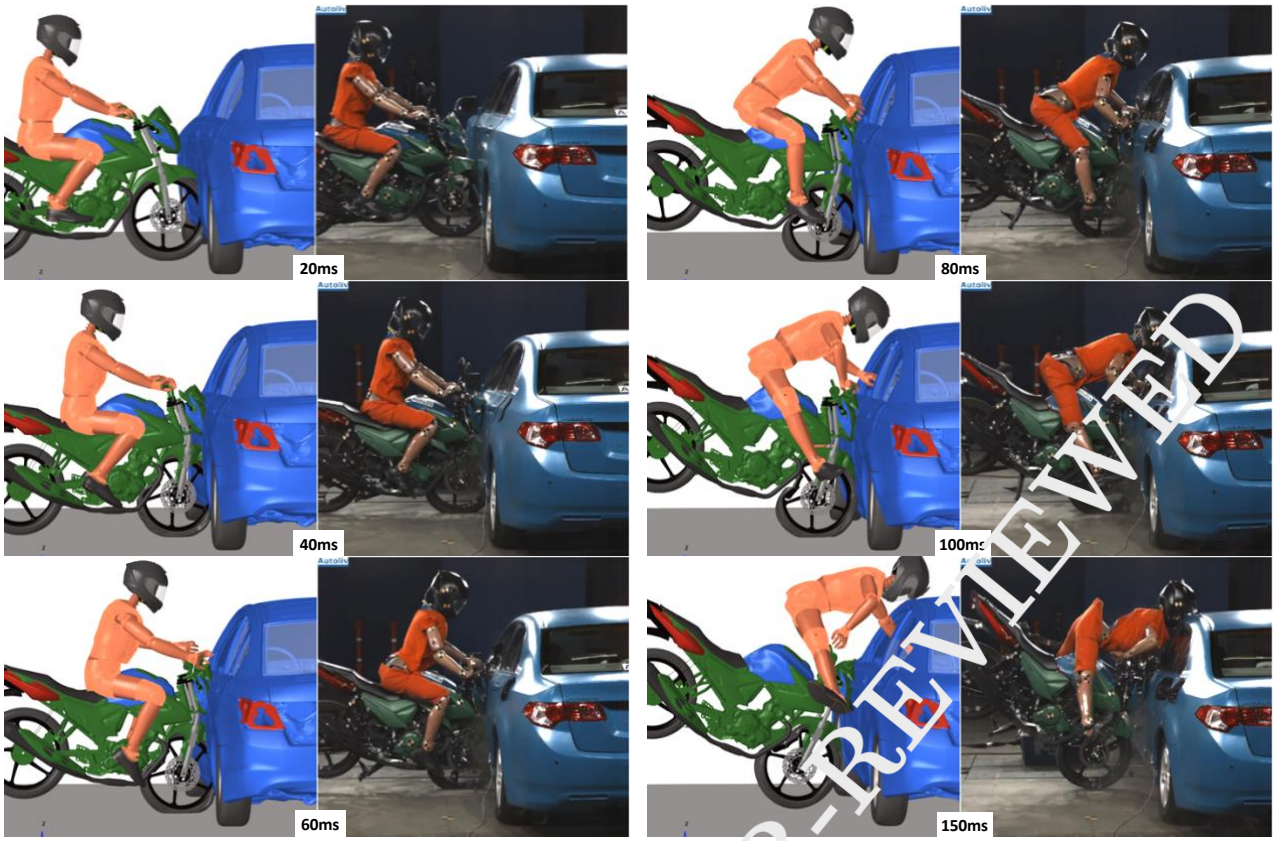

Figure 3.3 - Motion comparison between the computer model (left) and the full crash test (right)

Figure 3.4 – Comparison between test and simulation: the forks bending (left) and the front pipe deformation (right)

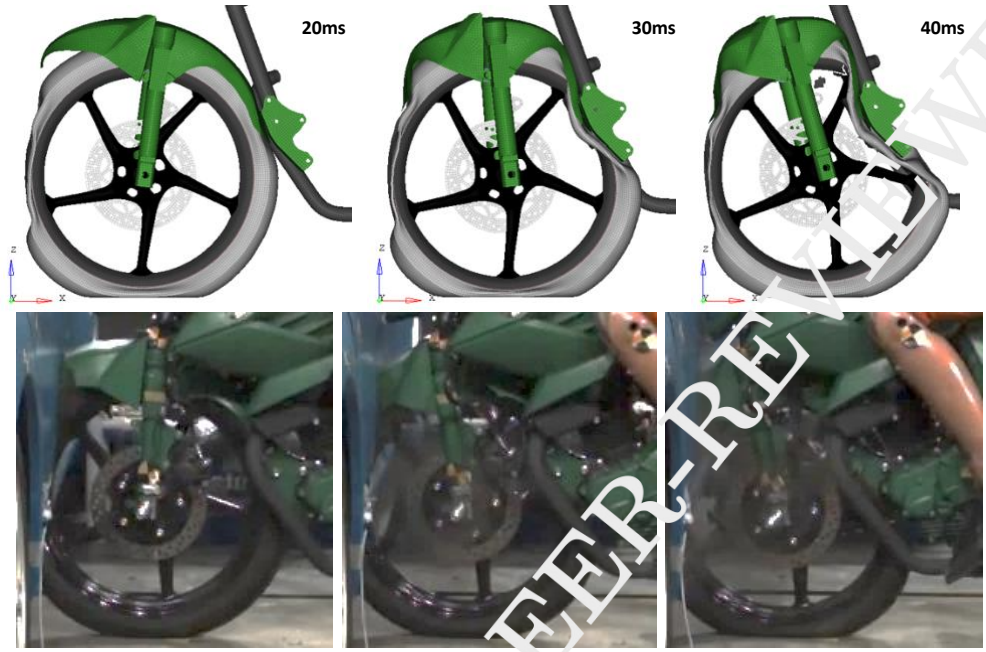

Figure 3.5 - Rim failure mechanism

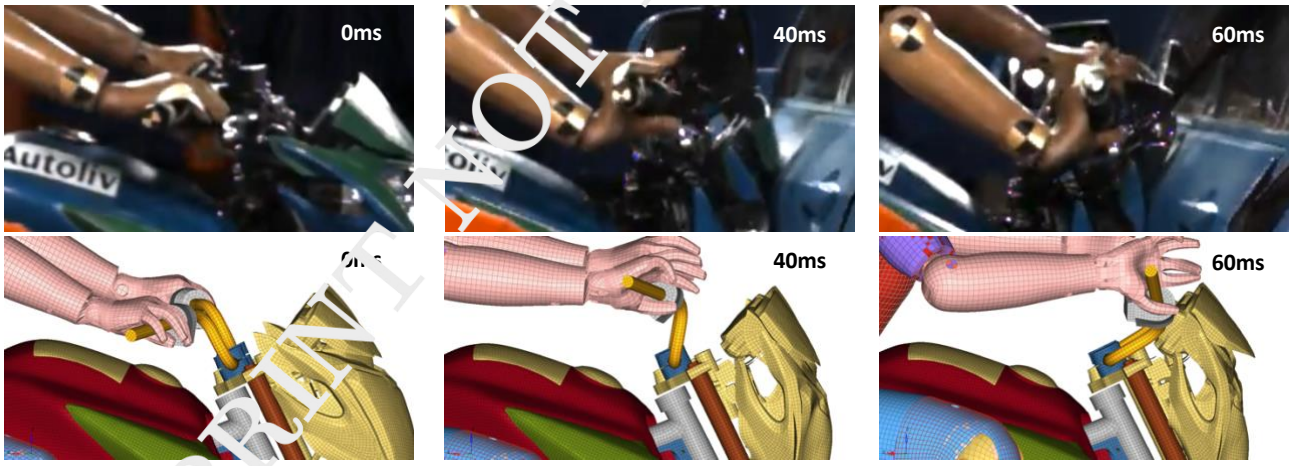

Figure 3.6 - Handlebar and headlamp rotation at collision

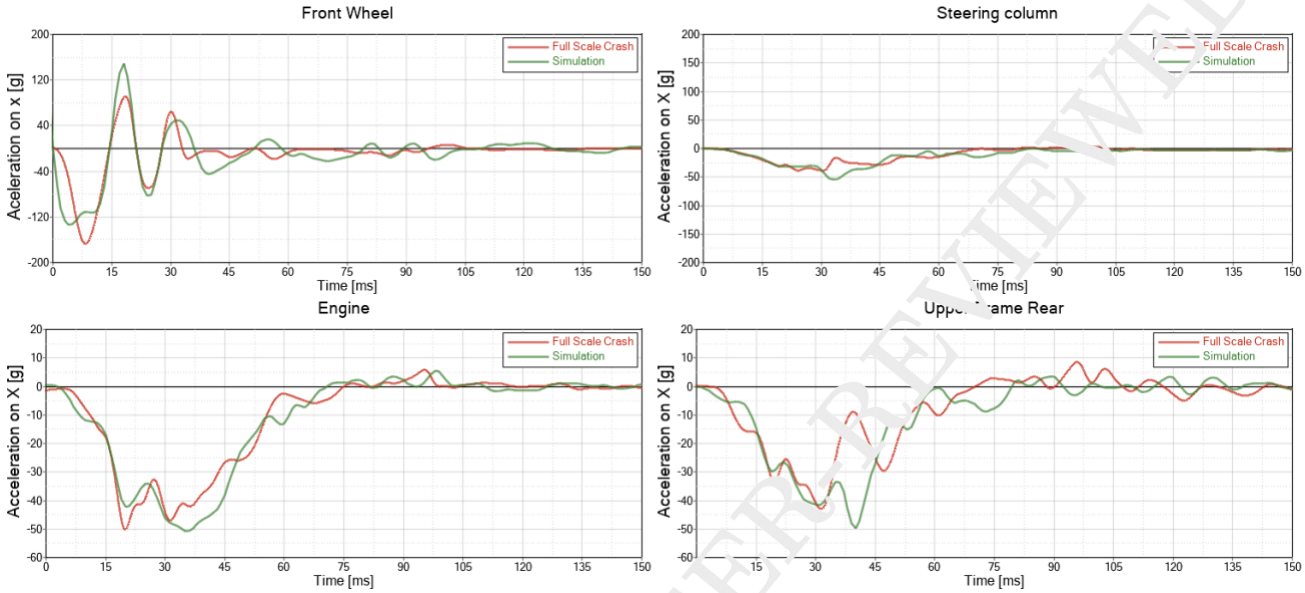

Figure 3.7 - The accelerations-time history measured at the front wheel, steering column, engine, and the rear of the upper frame from the full crash test (red) and the simulation (green)

4 Discussion

Although computer models have been used worldwide to simulate crash events for more than fifty years, no regulations are available to standardize modeling them. In addition, different techniques, such as multibody and finite element, require different precautions to be efficiently implemented. This study proposed a modeling guideline for a small-size PTW, observing which component played a significant role based on video and signal comparisons reported in chapter **Error! Reference source not found.**. Hereafter, they are discussed in chronological order, given their importance in replicating motorcycle dynamics and rider-to-motorcycle interactions.

The front wheel is the most critical part of a PTW frontal crash. It has been pointed out that the dynamic of the dummy depends initially on the collapsing characteristics of the front wheel [10]. A motorcycle wheel is usually made of a tire and the rim on which the tire is placed. Even though many cruiser motorcycles still use wire-spoke rims for appearance reasons [23], the vast majority of PTWs nowadays have alloy wheels fitted, like the Yamaha YS125 of this study. Although the rim typically possesses a high stiffness to transmit the power of the motorcycle with the lowest possible loss, on the other hand, it must provide, together with the tire, the maximum impact energy absorption to reduce the change of momentum imposed on the motorcycle [59]. The aluminum of the rim was calibrated in order to reproduce the failure noticed in both experimental tests. Generally, the rim can collapse on the front side, directly after contact with the obstacle, or on the back side at the beginning of the rebound, when the wheel rises while the motorcycle continues pushing forward. Thus, special attention was given to the failure parameter, also because casting aluminum alloys show, in general, brittle behaviors, with strain at failure between 0.03% and 0.07%. The pressure inside the tire is closely related to the failure of the rim. The implemented airbag formulation allowed catch the pressure increment caused by the volume reduction during the tire compression, as well as the sudden pressure drop when the rim failed. Since the tire is tubeless, which means no air chamber is between the carcass and the rim, the air spills out as soon as the rim breaks, resulting in a sudden drop in the tire pressure. If not appropriately modeled, the pressure inside can inflate back the tire and vigorously rebound the PTW with the dummy over it. In this regard, the initial tire profile should consider the effect of the pressure inside. It was not designed already all rounded as it was after the inflation but initially flatter and smaller. For this purpose, a proper scan of the carcass during the reverse engineering phase is recommended. Furthermore, it has been proved that minor modifications in a FE model can significantly affect dummy contact points and injury outcomes [32]. Therefore, there is a need to develop detailed PTW models that are geometrically accurate. Eventually, a correct assessment of the wheel orientation is crucial since the stiffness sensibly

changes depending on its first point of contact: e.g., the portion between two spokes will be necessarily weaker than the part on the top of the spoke. Therefore, after the two crash tests, the initial orientations of the wheel were changed accordingly to best match the initial test condition.
The second involved component is the front suspension. When riding, it is devoted to maintaining the wheel in contact with the ground and absorbing its asperities, but during a collision, it operates differently. Overall, a suspension spans three subsequent phases during a crash: the loading, the bending, and the rebounding phase. Once the front wheel enters the collision, the front suspensions are loaded. The compression length depends on the characteristic of the forks and the amount of load they receive. Whether they bottomed out or just compressed a few, the mass of the motorcycle behind the suspension continues pushing forward, causing plastic deformations on the shafts [14,17,60]. Material and thickness, which logically determine the stiffness of the shafts, primarily affected this phase. For this reason, one-dimensional representations of the suspensions [6,17] cannot be judged satisfactory in a frontal collision and should be rejected despite their capacity to reproduce the spring/damper response. From this point, the rebound of the suspensions starts (if they have not been gripped during the bending), and it tends to push the PTW backward, releasing the energy stored during the compression. Besides linear and rotational inertial forces, the three primary actions are provided by the spring force, the damping force, and the frictional force. As usual, the latter is tough to estimate as they depend on the material properties, geometrical tolerances, and the regime of lubrification. Therefore, it was decided to assume a coefficient for static friction. The spring forces are the most obvious in the system, and their contribution is the most important among the three. First, the total spring force created in telescopic front forks is more involved rather than the simple Hooke law. It is because there is a volume of air trapped inside the fork tubes that acts like an additional spring. The more the fork compresses, the more progressive the air spring becomes. Consequently, the front forks have two spring forces: the mechanical and the air spring force. For this reason, it was decided to compress the whole fork to measure the resultant spring rate, not dismounting the front suspension. In doing so, it is essential to remember that a third force is acting on the mechanism, the damping force, which, being viscous, depends solely on velocity rates. Therefore, a quasi-static test was ideal for measuring the spring rate without the contribution of the damping factor. Damping in modern motorcycle suspension components is created in several ways, but it almost always involves a fluid. The configuration can be as simple as forcing oil through a hole (as with the old-style damping rod forks in the Yamaha YS) or as sophisticated as a multi-stage, bending shim stack configuration combined with externally adjustable knobs. These several possible settings make it especially difficult to have a solid final answer on the damper response. For this reason, a range between 0.1 and 1.0 Ns/mm was evaluated in simulations with no substantial difference between the smallest and highest value.
After the front wheel and once the front forks bend, the third involved part is the headlamp. It can interact with the OV depending on either the PTW pitch or the extent of the fork bent [9,25], but in some cases, it can directly involve the rider, which rotates around the handlebar and makes head contact with the headlamp [6]. Hence, the headlamp should be considered when modeling a PTW [10]. Generally, the headlamp stiffness is relatively low due to the plastic material in which it is vastly made. On the other hand, the metal brackets on which it is bolted can develop a pretty high stiffness, especially if simplified in the computer model with rigid connections. The stiffening can lead to a different force propagation and make the PTW stuck toward a deformable opponent, like the lateral panel of the OV. Thus, a proper discretization of the bolts or at least cylindrical joints, such as in this study, can help prevent unreal motions and allow for the rotation of the headlamp when frontally loaded.
The dummy is not attached to the PTW, so the forces between them depend primarily on friction, which was proved to have a relatively large influence on dummy behavior [10]. This peculiarity applies especially to the fuel tank and the handlebar with which the rider interacts the most; hence they were the fourth and the fifth critical components in a frontal collision. During the crash, the handlebars typically show signs of rider contact, such as bending or forward rotation in the clamps [61]. This behavior was hardly replicable in the simulation since it largely depends on the exact geometry of the tight fit with which the handlebar is held inside the bolted clamps on the upper fork mount, Figure 2.4 (left). The cause of handlebar rotation is to be found in the interaction with the hand, and, in turn, their position was affected by the wrist and other joints till the shoulder; thus, the initial positioning of the dummy was reckoned essential to achieve correct motions. In the physical test, dummy hands are generally taped on the handlebar; sometimes, there are

different joint stiffnesses along the arms and fingers. As a consequence, the dummy may continue to hold on to the handle well after the PTW impacts the OV, leading to gaining additional height [16 18]. Depending on the dummy's characteristics, the hand grip was measured by other authors to vary between 50 N [36] and 250 N [16]. The Autoliv-Humanetics PTW v1.0.4 includes fingers on the dummy hands but no joints are allocated any specific stiffnesses. Nevertheless, the specific initial position (as described in paragraph 2) allowed prolonged contact of the hands on the handlebar in the computer simulation, thus, no further measures were implemented. Regarding the fuel tank, it is usually not directly involved in the crash against the OV, but it ends up deformed due to the interaction with the pelvis and the legs. For this purpose, the material parameters were tuned to visually reproduce the degree of deformation reported during the full crash test.

These five components were judged essential to adequately model a PTW for frontal collisions. Overall, the general motion, pitch, and rebound were replicated adequately (Figure 3.3). Similarly, the deformations (Figure 3.4, Figure 3.5, Figure 3.6) were consistent in magnitude and timing, with good agreement between the two models. The front wheel failure was replicated in the computer model, as well as the forks bending and the headlamp and handlebar rotation. Nevertheless, especially in the rigid barrier test, some discrepancy was seen in the acceleration, which was deplorable since the importance of a rigid barrier test, besides the fact it is recommended by the Standard [4], traditionally lay in the responses achievable with sensors ignoring external variabilities (e.g., the stiffness of the opponent vehicle (OV) or the effect of the dummy rider) [1,7,9–11,17,25,26,31,43,44,62–64]. The abovementioned discrepancies can be explained by knowing that, in the experimental test, a thin metal plate was placed on the front quarter of the wheel (connected to the hub laterally and the fender on top) to trigger the sensor acquisition system and to define time zero. Unfortunately, this implementation turned out to spoil the measurements made, especially for the peak values on the forks. In addition, in the test, the transducers were fastened with two bolts whose heads stayed out of the metal plate. The left one was partly hit by the front wheel, turning in an acceleration increment.

5 Conclusions

This paper showed how to develop an FE model of a small size motorcycle for frontal crashes by detailing structures that are typically critical to be replicated but crucial to produce a reliable motorcycle dynamic and rider-to-motorcycle interaction. Therefore, five critical components in the PTW were detailed: the front wheel, the front suspensions, the headlamp, the handlebar, and the fuel tank. The tire pressure and the suspension affect the way the PTW rebounds; the interaction of the engine bracket with the front rim determines the latter to break and the frame to deform; the tire failure and the fork bending affect the quantity of dissipated energy and, therefore, the PTW overall motion; the handlebar and headlamp rotation are the results of how the components are connected to the frame, and they affect the PTW pitch; the way the handlebar rotates and the fuel tank hinders the pelvis have significant effects on the final dummy height. In conclusion, it has been shown how to define a predictive PTW computer model for frontal crash applications from a reverse engineering process base. Observations on its fundamental parts have been made, and its predictive capability has been proved by two laboratory tests, which demonstrated high fidelity in reproducing accelerations, general motion, and main deformations. From this perspective, the obsolescence has been highlighted, at least in frontal collisions, of the ISO 13232 requirements in addressing the critical aspects of modeling vehicles for crash simulation.

ACKNOWLEDGEMENT
The authors would like to express their deepest gratitude to all the colleagues at Autoliv Research who contributed directly and indirectly to the completion of this research work. Their invaluable contributions and support have been instrumental in shaping this study. We especially express our sincere appreciation to Dr. J. Carroll and Dr. D. Barbani for their contribution with technical guidance and support.

Furthermore, we are grateful to Professors N. Lübbe and N. Baldanzini for providing the opportunity of developing this work under the agreement of an Erasmus+ Traineeship during the doctoral program of the corresponding author.

DISCLOSURE STATEMENT
No potential conflict of interest was reported by the authors.

FUNDING
No private or public fundings were received for this research.

REFERENCES

[1] D. Barbani, N. Baldanzini and M. Pierini, *Development and validation of an FE model for motorcycle-car crash test simulations*, International Journal of Crashworthiness 19 (2014), pp. 244–263.

[2] *Motorcycles — Test and analysis procedures for research evaluation of rider crash protective devices fitted to motorcycles — Part 1: Definitions, symbols and general considerations*. 2005.

[3] *Motorcycles — Test and analysis procedures for research evaluation of rider crash protective devices fitted to motorcycles — Part 6: Full-scale impact-test procedures*. Geneva Switzerland, 2005.

[4] *Motorcycles — Test and analysis procedures for research evaluation of rider crash protective devices fitted to motorcycles — Part 7: Standardized procedures for performing computer simulations of motorcycle impact tests*. 2005.

[5] A. Chawla, N.M. Rogers, J.W. Zellner and T. Nakatani, Methodologies for motorcyclist injury prediction by means of computer simulation, in Conference proceedings International Research Council on the Biomechanics of Injury, IRCOBI, 2004, pp. 207–218.

[6] A. Chawla, S. Mukherjee, D. Mohan, D. Bose, P. Rawat, T. Nakatani et al., *FE simulations of motorcycle-car frontal crashes, validations and observations*, International Journal of Crashworthiness 10 (2005), pp. 319–326.

[7] P. Bothwell, R.E. Knight and H.C. Petersen, *Dynamics of Motorcycle Impact*, Denver Research Institute/1971.

[8] A. Sporner, *Experimentelle und Mathematische Simulation von Motor-radkollisionen im Vergleich zum realen Unfallgschehen*, PhD Dissertation, TU München, 1982.

[9] J. Happian-Smith, M.A. Macaulay and B.P. Chinn, Motorcycle Impact Simulation and Practical Verification, in International Technical Conference on Experimental Safety Vehicles (ESV), 1987.

[10] A.L. Yettram, J. Happian-Smith, L.S.M. Mo, M.A. Macaulay and B.P. Chinn, Computer simulation of motorcycle crash tests, in International Technical Conference on the Enhanced Safety of Vehicles (ESV), 1994, pp. 1227–1240.

[11] J.J. Nieboer, J. Wismans, A.C.M. Versmissen, M.T.P. van Slagmaat, I. Kurawaki and N. Ohara, *Motorcycle crash test modelling*, SAE Technical Papers (1993), pp. 1–16.

[12] J.J. Nieboer, A.P. Goudswaard, J. Wismans, E.G. Jansseu and A.C.M. Versmissen, Computer simulation of motorcycle airbag systems, in International Technical Conference on Experimental Safety Vehicles (ESV), 1991, pp. 268–273.

[13] S.K. Kebschull, J.W. Zellner, R. van Auken and N. Rogers, Injury risk/benefit analysis of motorcyclist protective devices using computer simulation and ISO 13232, in International Technical Conference on the Enhanced Safety of Vehicles (ESV), 1998, pp. 2357–2374.

[14] Y. Wang and M. Sakurai, *Development and verification of a computer simulation model of motorcycle-to-vehicle collisions*, SAE Technical Papers (1999), pp. 1–18.

[15] S. Iijima, S. Hosono, A. Ota and Y. Takenori, Exploratory study of an airbag concept for a large touring motorcycle, in International Technical Conference on Experimental Safety Vehicles (ESV), 1998.

[16] S. Mukherjee, A. Chawla, D. Mohan, M. Singh, M. Sakurai and Y. Tamura, Motorcycle-car side impact simulation, in Conference proceedings International Research Council on the Biomechanics of Injury, IRCOBI, 2001.

[17] S. Mukherjee, A. Chawla, D. Mohan, M. Singh, M. Sakurai and T. Nakatani, Motorcycle-wall crash: simulation and validation, in Pam Users Conference Asia, 2000.

[18] A. Chawla and S. Mukherjee, *Motorcycle safety device investigation: A case study on airbags*, Sadhana 32 (2007), pp. 427–443.

[19] R. Canaple, G.P. Rungen, E. Markiewicz, P. Drazetic, J. Happian-Smith, B.P. Chinn et al., *Impact model development for the reconstruction of current motorcycle accidents*, International Journal of Crashworthiness 7 (2002), pp. 307–320.

[20] M. Deguchi, Modeling of a motorcycle for collision simulation, in International Technical Conference on the Enhanced Safety of Vehicles (ESV), 2003.

[21] M. Deguchi, Simulation of motorcycle-car collision, in International Technical Conference on the Enhanced Safety of Vehicles (ESV), 2005.
[22] S. Kanbe, M. Deguchi and Y. Hannya, Basic research for a new airbag system for motorcycle, in International Technical Conference on the Enhanced Safety of Vehicles (ESV), 2007.
[23] J.L. Wobrock, *MADYMO simulation, reconstruction, and biomechanical analysis of motorcycle crashes*, University of California, 2005.
[24] A.B. Ibitoye, R.S. Radin and A.M.S. Hamouda, *Roadside barrier and passive safety of motorcyclists along exclusive motorcycle lanes*, Journal of Engineering Science and Technology 2 (2007), pp. 1–20.
[25] H. Namiki, T. Nakamura and S. Iijima, *A computer simulation for motorcycle rider-motion in collision*, SAE Technical Papers (2003), pp. 1–8.
[26] H. Namiki, T. Nakamura and S. Iijima, A computer simulation for motorcycle rider injury evaluation in collision, in International Technical Conference on the Enhanced Safety of Vehicles (ESV), 2005.
[27] D. Barbani, N. Baldanzini, M. Pierini and M. Santucci, Analisi e sviluppo di un modello FEM di airbag integrato su motoveicolo, in 41st Convegno AIAS – Associazione Italiana per l'Analisi delle Sollecitazioni, 2012.
[28] A. Grassi, D. Barbani, N. Baldanzini, R. Barbieri and M. Pierini, Belted Safety Jacket: a new concept in Powered Two-Wheeler passive safety, in Procedia Structural Integrity, 8 (2018), pp. 573–593.
[29] N. Schulz, C.S. Dobrovolny and S. Hu'ebaus, Development of a finite element model of a motorcycle, in International LS-DYNA Users Conference, 2016.
[30] M. Mongiardini, B. Walton, R.H. Orzebieta, M. McKay, C. Menictas, A. Berg et al., Development of a motorcycle FE model for simulating impacts into roadside safety barriers, in First International Roadside Safety Conference, 2017, pp. 657–673.
[31] L. Berzi, N. Baldanzini, D. Barbani, M. Delogu, R. Sala and M. Pierini, Simulation of crash events for an electric four wheel vehicle, in Procedia Structural Integrity, 12 (2018), pp. 249–264.
[32] D. Barbani, N. Baldanzini and M. Pierini, *Sensitivity analysis of a FE model for motorcycle-car full-scale crash test*, SAE Technical Papers 2014-November (2014), pp. 1–8.
[33] T. Serre and M. Llari, Numerical analysis of the impact between a PTW rider and a car in different accident configuration, in IFMBE Proceedings, 31 (2010), pp. 521–524.
[34] R. Moradi and H.M. Lankarani, *A multi-body modeling and design of experiment investigation of a motorcyclist impact on roadside barriers at upright and sliding configurations*, ASME 2011 International Mechanical Engineering Congress and Exposition, IMECE 2011 7 (2011), pp. 697–705.
[35] Z. Xiao, L. Wang, F. Mo, X. Lv and C. Yang, *Influences of impact scenarios and vehicle front-end design on head injury risk of motorcyclist*, Accid Anal Prev 145 (2020), pp. 1–11.
[36] S. Xu, X. Jin, C. Luo and S. Fu, *Modeling method of rider-two-wheeler-road coupled system in two-wheeler traffic accident reconstrucitons*, International Journal of Crashworthiness (2021), pp. 1–9.
[37] B.O. Cherta, M. Llari, V. Honoré, C. Masson and P.J. Arnoux, *An evaluation methodology for motorcyclists' wearable airbag protectors based on finite element simulations*, International Journal of Crashworthiness 26 (2021), pp. 99–108.
[38] B.O. Cherta, M. Llari, S. Afquir, J.L. Martin, N. Bourdet, V. Honoré et al., *Analysis of trunk impact conditions in motorcycle road accidents based on epidemiological, accidentological data and multi-body simulations*, Accid Anal Prev 127 (2019), pp. 223–230.
[39] Q. Wang, Y. Lou, X. Jin, L. Kong, C. Qin and X. Hou, *Reverse reconstruction of two-wheeled vehicle accident based on Facet vehicle model and hybrid human model*, International Journal of Crashworthiness 27 (2022), pp. 661–676.
[40] S. Maier, L. Doléac, H. Hertneck, S. Stahlschmidt and J. Fehr, Evaluation of a novel passive safety concept for motorcycles with combined multi-body and finite element simulations, in Conference proceedings International Research Council on the Biomechanics of Injury, IRCOBI, 2020, pp. 250–265.

[41] T. Bonkowski, L. Hyncik and W. Lv, *PTW Passive Safety: Numerical Study of Standard Impact Scenarios with Rider Injury Risk Assessment*, SAE Technical Papers 2020-April (2020), pp. 1–27.
[42] Z. Xiao, L. Wang, Y. Zhang and C. Yang, *A study on motorcyclist head reponses during impact against front end of vehicle*, International Journal of Crashworthiness 27 (2022), pp. 147–159.
[43] P. V. Bhosale, Exploratory study on the suitability of an airbag for an Indian motorcycle using finite element computer simulations of rigid wall barrier tests, in International Technical Conference on Experimental Safety Vehicles (ESV), 2013.
[44] R. Moradi, S. Ramamurthy, C.K. Thorbole, P.S. Bhonge and H.M. Lankarani, Kinematic analysis of a motorcyclist impact on concrete barriers under different road conditions, in ASME 2010 International Mechanical Engineering Congress and Exposition, 2010.
[45] J. Carmai, S. Koetniyom and W. Hossain, *Analysis of rider and child pillion passenger kinematics along with injury mechanisms during motorcycle crash*, Traffic Inj Prev 20 (2019), pp. S13–S20.
[46] D. Setyanto, A.D. Soewono, A. Wibowo and R.T. Liong, *Design of a motorcycle frame at an automotive company in Indonesia*, International Journal of Engineering Research and Technology 13 (2020), pp. 738–743.
[47] International Transport Forum (ITF) and Organisation for economic co-operation and development (OECD), *Trends in Motorcycles Fleet*, 2008.
[48] V. Cossalter, *Motorcycle Dynamics Second Edition*, 2006.
[49] J. Phromjan and C. Suvanjumrat, *Optimized stress-strain ranges for hyperelastic constitutive models supporting the simulation of vertical stiffness on airless tire*, IOP Conf Ser Mater Sci Eng 1063 (2021), pp. 012002.
[50] R.R.V. Neves, G.B. Micheli and M. Alves, *An experimental and numerical investigation on tyre impact*, Int J Impact Eng 37 (2010), pp. 685–693.
[51] P. Baranowski, R. Gieleta, J. Małachowski and Ł. Mazurkiewicz, *Rubber structure under dynamic loading-computational studies*, Engineering Transactions 61 (2013), pp. 33–46.
[52] M. Cerit, *Numerical simulation of dynamic side impact test for an aluminium alloy wheel*, Scientific Research and Essays 5 (2010), pp. 2694–2701.
[53] M.H.R. Ghoreishy, *Finite Element Analysis of the steel-belted radial tyre with tread pattern under contact load*, Iranian Polymer Journal 15 (2006), pp. 667–674.
[54] E.O. Bolarinwa and O.A. Olatunbosun, Finite element simulation of the tyre burst test, in Proceedings of the Institution of Mechanical Engineers Part D Journal of Automobile Engineering, 2004, pp. 1251–1258.
[55] K.S. Tan, S. v. Wong and M.M.H.M. Ahmad, *Computational simulation of frontal impact of motorcycle telescopic fork*, International Journal of Crashworthiness 21 (2016), pp. 161–172.
[56] C. Moosbrugger, ed., *Atlas of Stress-Strain Curves*, 2nd ed.ASM International, 2002.
[57] J. Carroll, B. Boon, H. Sundmark, M. Burleigh and B. Li, A Powered Two-Wheeler Crash Dummy, in Conference proceedings International Research Council on the Biomechanics of Injury, IRCOBI, 2022.
[58] D. Pollard, D. Subit, J.P. Donlon and R.W. Kent, *Development of a computational framework to adjust the pre-impact spine posture of a whole-body model based on cadaver tests data*, J Biomech 48 (2015), pp. 636–643.
[59] K.S. Tan, S. v. Wong, R.S. Radin Umar, A.M.S. Hamouda and M.M.H. Megat Ahmad, *Experimental study on energy absorption characteristics of motorcycle front wheel-tyre assembly in frontal impact*, International Journal of Crashworthiness 11 (2006), pp. 131–142.
[60] J.W. Zellner, J.A. Newman and N.M. Rogers, Preliminary Research into the Feasibility of Motorcycle Airbag Systems, in International Technical Conference on Experimental Safety Vehicles (ESV), 1994.
[61] H.Jr. Hurt, J. Ouellet and D. Thom, *Motorcycle accident cause factors and identification of countermeasures*, Los Angeles, California, 1981.
[62] H. van Driessche, Development of an ISO Standard for Motorcycle, in International Technical Conference on Experimental Safety Vehicles (ESV), 1994.

[63] A. Chawla, S. Mukherjee, D. Mohan, S. Jasvinder and N. RIZVI, Crash simulations of Three wheeled Scooter Taxi (TST), in International Technical Conference on the Enhanced Safety of Vehicles (ESV), 2003.

[64] K.S. Tan, S. v. Wong and M.M.H. Megat Ahmad, *Development of high fidelity finite element model of motorcycle telescopic front fork*, International Journal of Simulation Modelling 15 (2016), pp. 436–449.